7-1-2004

Application of 3D Image Correlation Photogrammetry and Classical Photogrammetry to the Core-Drilling Method for Measuring In-Situ Stresses in Concrete Structures

Michael McGinnis

Stephen Pessiki

Hakan Turker

Application of 3D Image Correlation Photogrammetry and Classical Photogrammetry to the Core-Drilling Method for Measuring In-Situ Stresses in Concrete Structures

by

Michael McGinnis
mjmj@lehigh.edu

Stephen Pessiki
spp1@lehigh.edu

Hakan Turker
hturker@mku.edu.tr

ATLSS Report No. 04-16

July 2004

ATLSS is a National Center for Engineering Research on Advanced Technology for Large Structural Systems

117 ATLSS Drive
Bethlehem, PA 18015-4729

Phone: (610)758-3525
Fax: (610)758-5902

www.atlss.lehigh.edu
Email: inatl@lehigh.edu

TABLE OF CONTENTS

ACKNOWLEDGEMENTS

This research was funded by the Pennsylvania Infrastructure Technology Alliance. Additional support was provided by the Precast/Prestressed Concrete Institute, the Center for Advanced Technology for Large Structural Systems and by Lehigh University. Additional support for the photogrammetry measurements was provided by Trilion Quality Systems, of Pennsylvania and by Accurex Dimensional Measurement, of New Jersey. The support noted above is gratefully acknowledged.

LIST OF FIGURES

LIST OF TABLES

LIST OF SYMBOLS

a = hole radius

f'_c = concrete compressive strength

m = radius of measurement circle

r = distance of any point to center of hole

A, B, C, F, H, M, J = core-drilling material and geometric constants

E = modulus of elasticity

χ = material constant

μ = material constant

U = measured displacement

$\varphi(z), \kappa(z), \psi(z), \Phi(z), \Psi(z)$ = analytic functions of complex variable

A_n, a_k, a'_k = Fourier series coefficients

$\sigma_x, \sigma_y, \tau_{xy}$ = in-plane normal and shear stresses

K_x, K_y = in-plane stress gradients

α = angle measured counter-clockwise from the x-axis to the point of interest

u, v = radial and tangential relieved displacements

$\alpha_i, \beta, \theta_{ij}, \theta_{ji}$= geometrical parameters

ABSTRACT

A technique for the determination of in-situ stresses in concrete structures, referred to as the Core-Drilling Method, is presented. The method is similar to the ASTM Hole-Drilling Strain-Gauge Method except that the Core-Drilling Method is formulated in terms of displacement rather than strain. Measurements in the current work are performed with traditional photogrammetry, and the more novel (and more accurate) 3D Image Correlation Photogrammetry. The report reviews the background elasticity theory and discusses the results of verification experiments on steel plates.

CHAPTER 1

INTRODUCTION

1.1 INTRODUCTION

Reliable information about the in-situ state of stress in the concrete in an existing structure is often needed as part of the evaluation of the structure. The evaluation may be performed as part of the determination of the load rating for the structure, or to support a decision about the repair or replacement of the structure. As just one example, information about the in-situ state of stress in a prestressed concrete bridge girder can be used to estimate the effective prestress remaining in the girder. This information is useful in predicting the service load behavior and ultimate strength of the girder.

This report presents a summary of the theoretical background and the design and results of verification experiments for a nondestructive evaluation method to determine the state of stress in concrete in an existing structure. The method is referred to as the *Core-Drilling Method*[1, 2]. Potential applications of the method include the determination of in-situ stress in a variety of reinforced and prestressed concrete structures, including bridges, buildings, dams, retaining walls, tunnels, shafts, and containment vessels.

In the Core-Drilling Method, a circular core hole is cut in to the concrete in a structure, and the *displacements* that occur in the concrete as the hole is cut are measured. These measured displacements are then related to the in-situ state of stress in the structure. The proposed method is nondestructive since the ability of the structure to perform its intended function is not impaired and the core hole is repaired. The method is similar to the ASTM Hole-Drilling Strain Gauge Method (ASTM 837 1994) that consists of measuring *strains* at the surface of a specimen as a hole is drilled. The ASTM Hole-

Drilling Strain Gauge Method has been the subject of numerous technical publications, including methods to reduce the dependence of the calculations on material properties[3], to refine the techniques involved for calculation of non-uniform stresses through depth and utilize the advantages of finite element analysis[3-8], and to apply the technique to orthotropic materials[9]. The hole drilling strain gauge method is often used to determine residual stresses in homogenous materials such as metals. Its applicability to concrete structures is questionable because the heterogeneous nature of the concrete complicates strain measurement over small gauge lengths. The current research represents a novel use of a newer class of optical displacement measurement technique, namely 3D Image Correlation Photogrammetry[10]. A random pattern of dots is photographed on the specimen and by correlating the patterns within versions of the photographs taken before and after core drilling, deformation information is derived.

Figure 1.1 illustrates the proposed method. Three points, *i*, *j*, and *k* are shown on the surface of the test object. As the core hole is drilled, each point undergoes a *relieved displacement*, (*u* and *v*) relative to the center of the hole, where *u* and *v* are the radial and tangential components of the overall displacement respectively (additional information shown in Figure 1.1 will be discussed in the next section). Measured displacements are the relative displacement between any two of these three points, and are denoted with a capital *U*. These measured displacements are then related to the in-situ stresses in the structure prior to drilling the hole. In practice the location and number of measurement points is somewhat arbitrary. However, at least as many measurements as unknown stresses must be captured, and the measurement points should be located fairly close to the core hole to increase the magnitude of the observed displacements, and thus the accuracy of the technique. Any additional measurement points captured provide redundant data that can potentially be used to improve the accuracy of the technique.

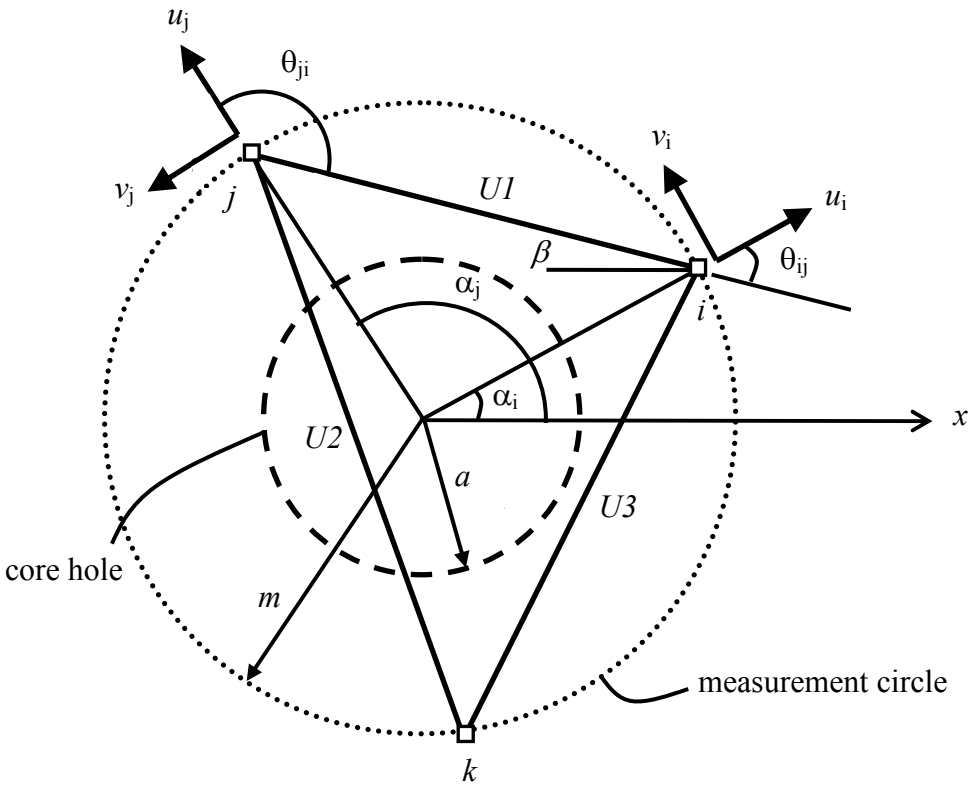

Figure 1.1: Illustration of the Core-Drilling Method showing displacement measurement between points *i* and *j*

CHAPTER 2

BACKGROUND

2.1 Development of Relieved Displacement Equations

Imagine that a core hole is drilled in a structure under stress and the hole surface is subjected to equal stresses as previously existed, as shown in Figure 2.1(a). The equilibrium of the body thus remains unchanged from prior to the hole drilling. In Figure 2.1(b), equal and opposite stresses to those on the hole surface of Figure 2.1(a) are applied at the core hole surface. The loading of Figure 2.1(b) can be superposed on Figure 2.1(a), resulting in the stress state after the hole is drilled, Figure 2.1(c). Thus the loading and corresponding displacements of Figure 2.1(b) are comparable to the relaxation caused by drilling the hole. In other words, the displacements caused by the loading in Figure 2.1(b) are the relieved displacements.

Elasticity methods treating a small through hole in an infinite, thin plate are be used to determine the relationship between the loads and displacements of Figure 2.1(b). Assumptions made in the derivations presented here are that the material is linear elastic, isotropic, homogenous, and that the load is distributed uniformly through the plate thickness. The problem is treated as a two dimensional problem of linear elasticity and solved for plane stress and plane strain assumptions, similar to the approach of the ASTM Hole-Drilling Strain Gauge Method excepting that displacements, rather than strains are the quantities of interest. Turker and Pessiki (2003)[2] incorporates finite elements to investigate the validity or consequences of many of these assumptions, such as the effects of non-through holes, the effects of plates of finite size, and the effects of stresses that vary though the thickness of the plate.

This report treats two related stress states in the plane of the plate, Case 1 and Case 2 of Figure 2.2. Case 2 shows a stress state that is linearly varying in-plane, with constant shear stresses. Case 1 degenerates from Case 2 if the normal stress gradients are taken to be zero. Derivations for Case 1 are presented in detail herein, for Case 2 a summary is presented; the interested reader is directed to Turker and Pessiki (2003)[2].

The two dimensional elasticity problem is solved using the potential function of complex method as outlined by Muskhelishvili[11]. The governing bi-harmonic equation for an isotropic material

$$\nabla^4 U = \frac{\partial^4 U}{\partial x^4} + 2\frac{\partial^4 U}{\partial x^2 \partial y^2} + \frac{\partial^4 U}{\partial y^4} \tag{2.1}$$

can be solved by finding a bi-harmonic function, *U(x,y)* that satisfies the boundary conditions. If *U(x,y)* is expressed in terms of analytic functions of complex variable

$$U(x,y) = \Re[\bar{z}\varphi(z) + \kappa(z)] \tag{2.2}$$

then Muskhelishvili's displacement and stress equations for a polar coordinate system are given as

$$2\mu(u+iv) = e^{-i\alpha}[\chi\varphi(z) - z\overline{\varphi'(z)} - \overline{\psi(z)}] \tag{2.3}$$

$$N - iT = \Phi(z) + \overline{\Phi(z)} - e^{2i\alpha}[\bar{z}\Phi'(z) + \Psi(z)] \tag{2.4}$$

where

$$\varphi(z) = \int \Phi(z)dz$$

$$\psi(z) = \int \Psi(z)dz = \frac{d\kappa}{dz}$$

With static equilibrium, in can be shown that for Case 1, the stresses around any circle are

$$\sigma_s = \frac{\sigma_x - \sigma_y}{2} \sin 2\alpha - \tau_{xy} \cos 2\alpha \tag{2.5}$$

$$\sigma_n = \frac{\sigma_x + \sigma_y}{2} + \frac{\sigma_x - \sigma_y}{2} \cos 2\alpha + \tau_{xy} \sin 2\alpha \tag{2.6}$$

The tractions, N and T, around the core hole can also be expressed in complex Fourier expansion as

$$N - iT = \sum_{-\infty}^{\infty} A_n e^{-in\alpha} \tag{2.7}$$

where the constants A_n are found by equating terms of like exponents with their counterparts in Equations (2.5) and (2.6), assuming that the tractions applied to the hole are the inverse of the stresses expressed in Equations. (2.5) and (2.6). For Case 1, the constants determined are

$$\begin{aligned} A_0 &= -\frac{\sigma_x + \sigma_y}{2} \\ A_2 &= -\frac{\sigma_x - \sigma_y}{2} + i\tau_{xy} \end{aligned} \tag{2.8}$$

all other $A_n = 0$.

With complex Fourier series expansion, $\Phi(z)$ and $\Psi(z)$ for a region bounded by a circle are written as

$$\Phi(z) = \sum_{0}^{\infty} a_k z^{-k}$$
$$\Psi(z) = \sum_{0}^{\infty} a'_k z^{-k} \tag{2.9}$$

The constants a_k and a'_k are determined from the boundary conditions on the core hole circle and at infinity.

Using Equation (2.7) to express the boundary condition on the hole (tractions are equal to the *N*-*iT* derived) and knowing that at infinity the stresses should be zero, the coefficients of Equation (2.9) can be determined by equating terms with like powers of *z*. The coefficients thus determined are

$$a_2 = \left[-\left(\frac{\sigma_x - \sigma_y}{2} \right) - i\tau_{xy} \right] a^2$$
$$a'_2 = \left(\frac{\sigma_x + \sigma_y}{2} \right) a^2 \tag{2.10}$$
$$a'_4 = -3a^4 \left[\left(\frac{\sigma_x - \sigma_y}{2} \right) + i\tau_{xy} \right]$$

All other a_k, a'_k=0

With φ(*z*) and ψ(*z*) now fully defined, Equation (2.3) is applied to yield relieved displacements of

$$u = \left(\frac{\sigma_x + \sigma_y}{2} \right) A + \left(\frac{\sigma_x - \sigma_y}{2} \right) B \cos 2\alpha + \tau_{xy} B \sin 2\alpha \tag{2.11}$$

$$v = \left(\frac{\sigma_x - \sigma_y}{2} \right) C \sin 2\alpha - \tau_{xy} C \cos 2\alpha \tag{2.12}$$

where

$$A = \frac{a^2}{2\mu r}$$
$$B = \frac{a^2[r^2(1+\chi) - a^2)]}{2\mu r^3}$$
$$C = \frac{a^2[r^2(1-\chi) - a^2)]}{2\mu r^3}$$

Relieved displacements give the displacement of a point relative to the center of the through-hole. However, in practice, a displacement measurement might be taken between two points, neither of which is the center of the hole. Figure 1.1 shows a displacement measurement of this type. The measured displacement between the two measurement points, *i* and *j* is defined in terms of relieved displacements as follows:

$$U = u_i \cos\theta_{ij} - v_i \sin\theta_{ij} - u_j \cos\theta_{ji} + v_j \sin\theta_{ji} \tag{2.13}$$

where

$$\theta_{ij} = \alpha_i + \beta$$
$$\theta_{ji} = \alpha_j + \beta$$
$$\beta = \pi - (\alpha_i + \alpha_j)/2$$

2.2 Determination of In-Situ Stress Equations

To solve for the 3 unknown stresses of Case 1 (σ_x, σ_y, τ_{xy}) or the 5 unknowns of Case 2 (σ_x, σ_y, τ_{xy}, K_x, K_y), 3 and 5 measured displacements respectively are required. 3 (or 5) equations expressing measured displacements in terms of in-situ stresses must be solved simultaneously for the unknown stress quantities. In this report, the two measurement configurations shown in Figure 2.3 were used. All measurement points (shown with squares) are located on a fictitious measurement circle (shown dotted) some distance from the edge of the core hole (shown dashed). The measured displacements between

two points are shown with solid lines in the figure. Using Equations (2.11) and (2.12), the measured displacements for Case 1, Configuration A are as follows:

$$U1 = A(\sigma_x + \sigma_y) + B(\sigma_x - \sigma_y) \tag{2.14}$$

$$U2 = A(\sigma_x + \sigma_y) + 2B\tau_{xy} \tag{2.15}$$

$$U3 = A(\sigma_x + \sigma_y) - B(\sigma_x - \sigma_y) \tag{2.16}$$

Equations (17)-(19) are solved simultaneously for in-situ stresses resulting in:

$$\sigma_x = \frac{A(U1 - U3) + B(U1 + U3)}{4AB} \tag{2.17}$$

$$\sigma_y = \frac{A(-U1 + U3) + B(U1 + U3)}{4AB} \tag{2.18}$$

$$\tau_{xy} = \frac{-U1 + 2U2 - U3}{4B} \tag{2.19}$$

The process outlined above (Equations (2.5)-(2.19)) for the Case 1 stress state with Configuration A is repeated for the Case 2 stress state in conjunction with Configuration B. The resulting relieved displacement and in-situ stress equations are

$$\begin{aligned} u = {} & \left(\frac{\sigma_x + \sigma_y}{2}\right)A + \left(\frac{\sigma_x - \sigma_y}{2}\right)B\cos 2\alpha + \tau_{xy}B\sin 2\alpha \\ & + K_x(F\sin\alpha + H\sin 3\alpha) + K_y(-F\cos\alpha + H\cos 3\alpha) \end{aligned} \tag{2.20}$$

$$\begin{aligned} v = {} & \left(\frac{\sigma_x - \sigma_y}{2}\right)C\sin 2\alpha - \tau_{xy}C\cos 2\alpha \\ & + K_x(M\cos\alpha + J\cos 3\alpha) + K_y(M\sin\alpha - J\sin 3\alpha) \end{aligned} \tag{2.21}$$

$$\sigma_x = \frac{\sqrt{2}}{8AB}\left[A(U1 - U2 - U3 - U4 + 2\sqrt{2}U5) + B(-U1 + U2 + U3 + U4)\right] \quad (2.22)$$

$$\sigma_y = \frac{\sqrt{2}}{8AB}\left[A(-U1 + U2 + U3 + U4 - 2\sqrt{2}U5) + B(-U1 + U2 + U3 + U4)\right] \quad (2.23)$$

$$\tau_{xy} = \frac{\sqrt{2}}{8C}\left[U1 + U2 - U3 + U4\right] \quad (2.24)$$

$$K_x = \frac{\sqrt{2}}{4(F - H - M - J)}\left[U1 + U2 + U3 - U4\right] \quad (2.25)$$

$$K_y = \frac{\sqrt{2}}{4(F - H - M - J)}\left[U1 - U2 + U3 + U4\right] \quad (2.26)$$

where A, B, and C are as before (Equation (2.13)), and

$$F = \frac{a^4}{16\mu r^2}$$

$$H = \frac{a^4}{16r^4}\left[r^2(\chi + 2) - 2a^2\right]$$

$$M = -F$$

$$J = \frac{a^4}{16r^4}\left[r^2(\chi - 2) + 2a^2\right]$$

2.3 Review and Evaluation of Displacement Measurement Techniques

Roughly speaking, the typical magnitude of displacement that must be measured in a concrete structure subject to the testing with Core-Drilling Method is about 10-20 μm. With this magnitude of displacement providing context, existing displacement measurements techniques were reviewed to evaluate their applicability to the Core-

Drilling Method. The measurement techniques that were reviewed are broadly grouped in to three categories: (1) contact measurement techniques; (2) full field optical measurement techniques; and (3) discrete point optical techniques. A summary is given below.

Examples of contact measurement techniques include DEMEC (demountable mechanical strain gauges) gauges, LVDT (linear variable differential transformers), and vibrating wire strain gauges, to name a few. Resolution of a DEMEC gauge is reported to be as low as 1-2 μm, depending on the gauge length. Theoretically, the resolution of an LVDT is infinite, but in practice the resolution is limited by the electronic equipment employed in the measurement system. While these and other contact measurement techniques may be able to provide the required measurement resolution, each requires hard mounting of the measurement device to the stressed specimen prior to core hole drilling. These types of approaches may be feasible in a controlled laboratory environment, but under field conditions the difficulty in achieving consistent measurement fidelity is considerably magnified. Several researchers[11-12] have performed investigations into in-situ stresses with methods similar to the Core-Drilling Method using vibrating wire strain gauges and DEMEC gauges to achieve reported accuracy of approximately ± 10 percent in the laboratory but *considerably* less accuracy in field trials.

Optical techniques that take advantage of the interference properties of light waves were included in the category of full field optical measurement techniques. Examples of such techniques include holographic interferometry, speckle interferometry and shearography. While these methods would likely work well in the laboratory with the Core-Drilling Method, these methods are not proposed for this research because the objective is to develop a method that will eventually be applicable in the field. The optical techniques cited above can be sensitive to environmental factors such as vibration, and in some cases to rigid body motion, so they may be limited in field use for this particular application.

Examples of discrete point optical techniques include Photogrammetry and 3D Image Correlation Photogrammetry. Both techniques are non-contact in nature and measure

location of discrete points on the surface of the measured object. Photogrammetry involves placing physical targets on the object and determining their locations. Image Correlation Photogrammetry combines photogrammetric principles with the rapidly maturing techniques of image correlation. Due to their relative cost, accuracy, ease and speed of use, and field applicability and portability, these techniques hold great promise for use with the Core-Drilling Method and their suitability is evaluated in the current work.

Photogrammetry is a three-dimensional coordinate measurement technique that is widely accepted in industrial applications. Based on triangulation principles, photogrammetry uses a series of photographs taken of the measured object from numerous angles to recreate the three-dimensional coordinates of the targets that are placed on the object. With many different views of each target, the exact location of the target can be triangulated. This triangulation depends on knowledge of the camera's position and orientation for each photograph that is analyzed. The three major analytical functions that must be performed to analyze photogrammetric data are: (1) triangulation; (2) resection; and (3) self-calibration of the camera to eliminate errors such as those due to lens and camera imperfections, temperature and humidity effects, etc. Each function is described below.

To *triangulate* the position of a target in a series of photographs, the x, y location of the point in each photograph is measured. An object with known scale is included in each photograph for this purpose. In practice this is typically done by placing a simple scale bar or cross on the object. If the camera location and aiming direction for each photograph is known, the theoretical lines from the camera positions to the target can be intersected to produce the target's three-dimensional location.

The process of determining the camera's position and aiming direction (collectively hereafter referred to as the camera's orientation) is called *resection*. In the resection process, the known x, y, z coordinates of several well-distributed targets within a

particular photograph are used to determine the orientation of the camera for that particular photograph.

Self-calibration of the camera relies on the availability of photographs taken from a variety of camera orientations with numerous well-distributed targets captured in each image. These are characteristics that are always present in a well planned photogrammetric survey, as they also aid the mathematical accuracy of the triangulation and resection steps.

It is clear that triangulation and resection are interrelated, i.e. triangulation requires known orientation to calculate location and resection requires known location to get orientation. Thus the simultaneous solution of the governing geometric equations from all three phases is required. *Bundle adjustment* is the term used to describe the mathematical process whereby triangulation, resection and self-calibration are performed simultaneously to determine the precise three-dimensional location of the target points with a minimum amount of error (typically with a root-mean-square approach). A quality photogrammetric survey can yield accuracy in coordinates of approximately 25 μm. However, typical surveys are of areas usually larger than several square meters. Close range photogrammetry has the potential to improve this resolution by an order of magnitude or better.

3D Image Correlation Photogrammetry (3D ICP) combines techniques of image correlation with the photogrammetric location principles described above. Image correlation is possible only with the advent of high-speed computers. Image correlation algorithms mathematically engage in pattern recognition. In Image Correlation Photogrammetry, a fairly fine pattern with good contrast (such as would be created with 'spluttering' spray paint) is applied to the measured object. The pattern will then deform with the object under load. The object is captured in a pair of high quality cameras while it is loaded. With image processing software, unique sub-regions called facets of the applied pattern are identified and tracked. These facets can be tracked with sub-pixel accuracy. Three-dimensional locations of these facets are tracked as load is applied,

yielding displacements. Tracking the dense cloud of points within the applied pattern provides displacement information that is 'near' full field. The resolution of the technique is expressed in terms of strain and is approximately 10-20 micro-strain with older generation cameras and as much as 4 times better with newer cameras. The displacement resolution of this technique then scales somewhat linearly with the area to be measured. For example, with newer cameras (4 mega pixels) over a square area that measures 0.25m x 0.25 m, displacement resolution is about 1-2 μm.

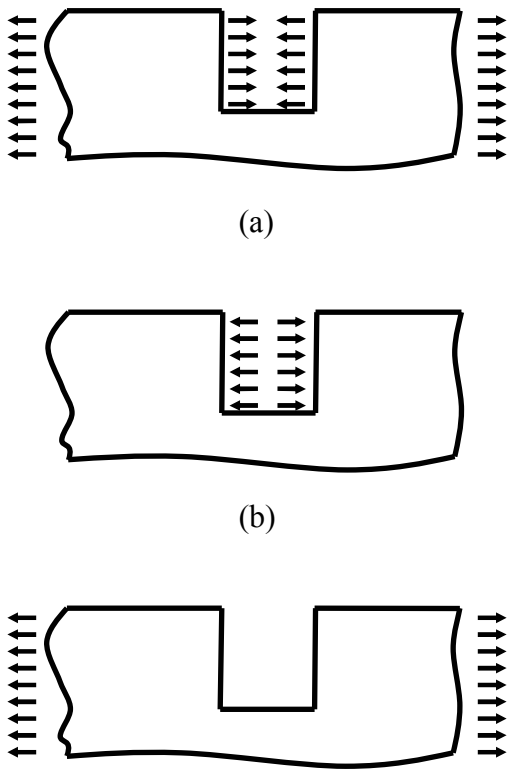

Figure 2.1: Superposition of loading to find relieved displacement caused by drilling a core hole: (a) original stress; (b) relieved in-situ stresses; (c) final stress

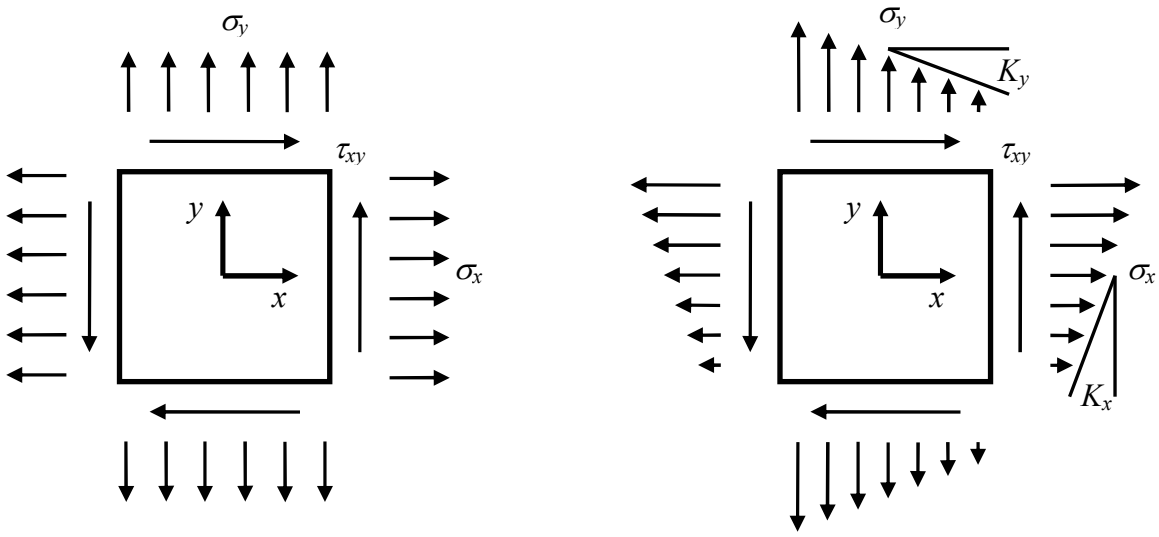

(a) (b)

Figure 2.2: Stress states treated in the Core-Drilling Method: (a) uniform normal and shear stress; (b) biaxial linear normal stress gradient and uniform shear stress

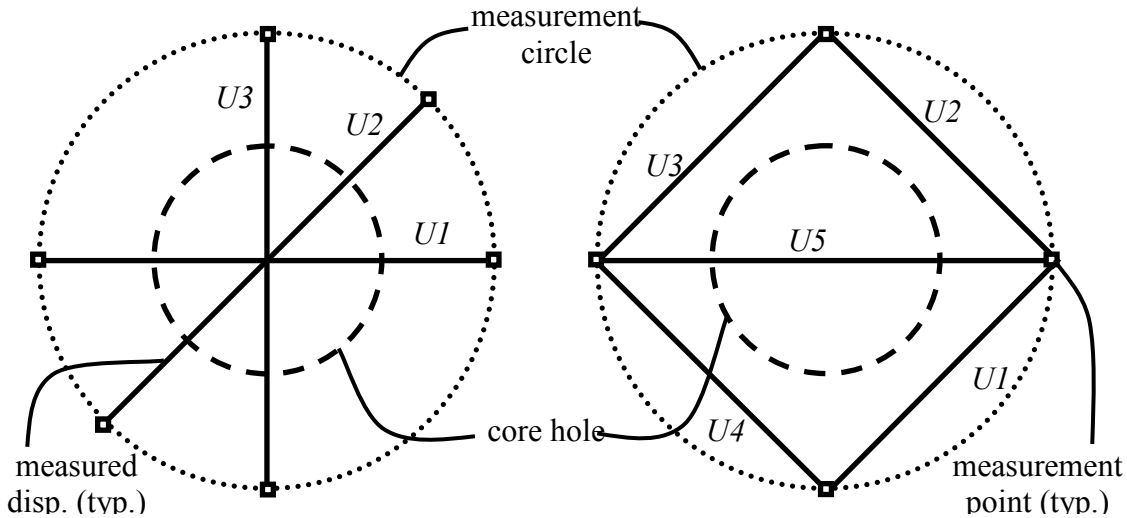

Figure 2.3: Measurement configurations: (a) Measurement Configuration A; (b) Measurement Configuration B

CHAPTER 3

VERIFICATION EXPERIMENTS

3.1 Experimental Overview

Three steel plates were tested in tension in these experiments, as shown schematically in Figure 3.1. Plates 1 and 3 were loaded in concentric axial tension with a force P to generate a uniform stress field, Plate 2 was loaded with a similar axial load in eccentric tension at the kern point to generate a stress field that theoretically varies linearly from zero on one edge of the plate to twice the nominal value at the opposite edge.

The geometry and axial load P applied to Plate 1 was designed to match the relieved displacements in a hypothetical concrete specimen with an in-situ uni-axial compression stress of 13.8 MPa. Steel was used instead of concrete to provide a specimen with known elastic modulus and to allow the test to be performed in tension instead of compression, thereby simplifying the verification experiment. The steel used was HPS 100, with an assumed modulus of elasticity, E of 200 GPa and an assumed yield stress of 690 MPa. Steel with a relatively high yield point was chosen to ensure that the loads applied to the plate as magnified by the stress concentration around a core hole would not induce yielding in the central region of the specimens. Table 1 shows a test matrix with the pertinent geometric, material, and load data for Plates 1, 2 and 3, and the hypothetical concrete structure considered. Figure 3.2 shows the anticipated radial (u) and tangential (v) displacements for the hypothetical concrete structure and the steel test specimen used to represent the hypothetical concrete structure.

3.2 Experimental Details

An arrangement of bonded wire strain gauges were affixed to each side of each plate to verify the expected in-plane normal stress quantities and stress gradients and to verify

that there was not undue out-of-plane bending of the plate. Figure 3.4 shows the layout of these strain gauges for each plate, as well as the numbering scheme for the gauges. The gauges for the front face of Plate 1 are also visible in Figure 3.3. Measurements Group Inc. model CEA-06-250UN-350 350 ohm resistance gauges with a gauge factor of 2.05 were used in conjunction with a series of Vishay 2120A strain gauge conditioner and amplifier systems. The gain and excitation voltage of the system were set so that the output readings were analogous to stress readings in the plates in units of psi/10; however, stresses in this report are always presented in units of MPa. The gain and excitation voltage settings of the instrumentation system are provided with the output tables for each plate. A load cell was incorporated into the load path to measure load. The load cell was calibrated using a SATEC 600 kip loading machine and a FLUKE 8840A voltmeter. The calibration data for the load cell is presented in Table 2 and Figure 3.5.

Figure 3.3 shows the load frame used to test the two plates, with Plate 1 positioned in the frame. The plates were gripped at each end by a clevis with a single load pin and loaded at one end with a hydraulic jack. The length of the plates was chosen to ensure that the load was well distributed in the center test region of each plate. Edge effects were avoided by ensuring that the plate width to core hole diameter ratio was greater than a specified limit[2]. Prior to testing, each plate was loaded to approximately 125% of the tested load a minimum of 3 times. The residual offset in the strain gauge readings prior to these preliminary loading steps were minimal, and the gauges were re-zeroed prior to final loading. Prior to taking a displacement reading, the hydraulic pump was turned off (but left pressurized to maintain load).

3.3 Experimental Results

Tables 3-5 contain the strain gauge and load cell data for each of the three plates. Figures 3.6-3.8 show the stresses at each gauge location plotted versus load for each of the plates. Note that the front face gauges are plotted with a dotted line and the back face gauges with a solid line. Further, each set of gauges that were affixed back-to-back (as for example gauges 1 and 7) share the same symbol. The data plotted in this manner allows

the presence of in-plane (strong axis) bending and out-of-plane (weak axis) bending to be detected. For Plates 1 and 2, there is little out-of-plane bending present. Figure 3.8 shows the presence of more significant out-of-plane bending in Plate 3. This is illustrated by the distinct separation between the stress readings on the front face of the plate (shown dashed), and the back face of the plate (shown solid). The difference in stress between front and back face shows classic through-thickness bending and is most prominent in Plate 3. Figures 3.9-3.11 show the final stress values for each plate plotted versus the horizontal location across the plate, to clearly show the stress profile across each plate. Again, these plots allow for the detection of strong and weak axis bending. A best-fit linear regression through the data of each figure (3.9-3.11) results in the stress and gradient values for each plate as reported in Table x, with the exception that the gradient for Plate 1 (0.042 MPa/mm) and Plate 3 (0.015 MPa/mm) have been neglected.

Figure 3.12 shows photographs of two of the plates after coring. Figure 3.12(a) is Plate 1 subjected to traditional Photogrammetry, and Figure 3.12(b) is Plate 2 subjected to 3D Image Correlation Photogrammetry. Plate 3 was similar in appearance to Plate 2. Shown in these photographs are the manually placed discrete targets used in the traditional photogrammetry, and the 'spluttered' spray paint applied for the 3D Image Correlation photogrammetry. Each plate was loaded as described above. A reading was taken with the given displacement measurement technique, and then a core hole was cut in the plate. The coring operation was performed with a magnetically attached drill, as shown in Figure 3.13. After coring, the load was returned to the value immediately prior to coring (coring slightly 'softens' the plate structure, resulting in a subsequent drop in load). After this step, a second reading was taken to determine the relieved displacements. The load and stress values immediately prior and immediately subsequent to coring along with the averages of the two are presented in Tables 4 and 5 for Plates 2 and 3. In Table 3, only the average values for Plate 1 are shown.

Figure 3.14 compares the measured displacements with the theoretical displacements from all three plates. In the figure, rigid body motions have been removed from each measured displacement quantity. For Plate 1, the measurement radius considered was 42

mm, for Plates 2 and 3, 44 mm. 3D Image correlation photogrammetry provided displacement values for thousands of discrete points on the surface of the plate, only a few are shown here. Further consideration of the richness of this data set beyond that considered here would almost certainly improve the accuracy of the stress measurements presented in the following section. In general, good agreement is obtained between the measured and theoretical displacements. This suggests that the two measurement techniques provide acceptable accuracy for the problem of interest (stresses in concrete).

Equations (17)-(19) and (22)-(26) were applied to Plates 1, 2 and 3 as appropriate to determine the in-situ stress in each plate. Table 6 shows the measured stress quantities for each plate tested as well as the relative error between the measured quantity and that applied. In each case, the measured values are the results of averaging the stress values obtained from Configuration A or B every 15 degrees around the measurement circle.

3.4 Discussion of Results

For the Plate 1 test, the calculated stress results are within 17% of the applied stress quantities, encouraging for a first test of the technique. In an actual field test on a concrete structure, the modulus of elasticity, E, of the concrete would be determined from the core taken and would likely be determined within 10-15%, so these results are certainly within this uncertainty range. Further, as this was the first use of traditional photogrammetry for this application, the targets were placed manually, resulting in a certain amount of relative positional error that was not accounted for in the equations as currently conceived. A simple, pre-fabricated target array that could be affixed to the specimen would likely improve the accuracy of the technique.

For Plate 2, excellent results (less than 7% error in normal stress) were obtained with 3D Image Correlation Photogrammetry. The reason for the relatively high error in the calculation for K_x is unknown at this time and warrants further study. One possibility is that the relative magnitude of the relieved displacements due to the bending (linear gradient) portion of the applied stress field is significantly smaller than that for the normal (constant) portion of the applied stress field, and thus the linear gradient terms are

more difficult to capture experimentally. As stated previously, 3D ICP captures thousands of points, however here only a relative scarcity (<30) points were used to perform the in-situ stress calculations. It is likely that a numerical scheme involving a much larger subset of the available data (as for example that proposed by Schajer and Steinzig[14]) would increase the accuracy in the K_x predictions.

For Plate 3, the accuracy in stress results was not as anticipated. Plate 3 was the first plate tested, and there were issues with the coring technique. Lubricating oil was not used while coring this plate, resulting in a prolonged drilling time and perhaps exceptional heating of the material immediately surrounding the core hole. For coring the other two plates, lubricating oil was used. Further, as mentioned previously, there was significant out-of-plane bending present in the Plate 3 test that was unaccounted for in the in-situ stress equations as applied. Perhaps application of the incremental formulation of the Core-Drilling Method[2] would yield better results; that effort is left for future study.

It has been shown in the current report that photogrammetry and 3D Image Correlation Photogrammetry are robust enough to capture the expected displacements involved in a typical concrete structure subjected to the Core-Drilling Method. Current work investigates some of the further complications of the technique as applied to concrete, among them:

- Allowance for moisture induced deflections (e.g. swelling from moisture uptake during the wet coring process, and shrinkage due to concrete drying and carbonation),
- Allowance for changes in expected stress distributions due to creep and the presence of steel reinforcement, and
- The influence of coarse aggregate size, gradation, and volume fraction.

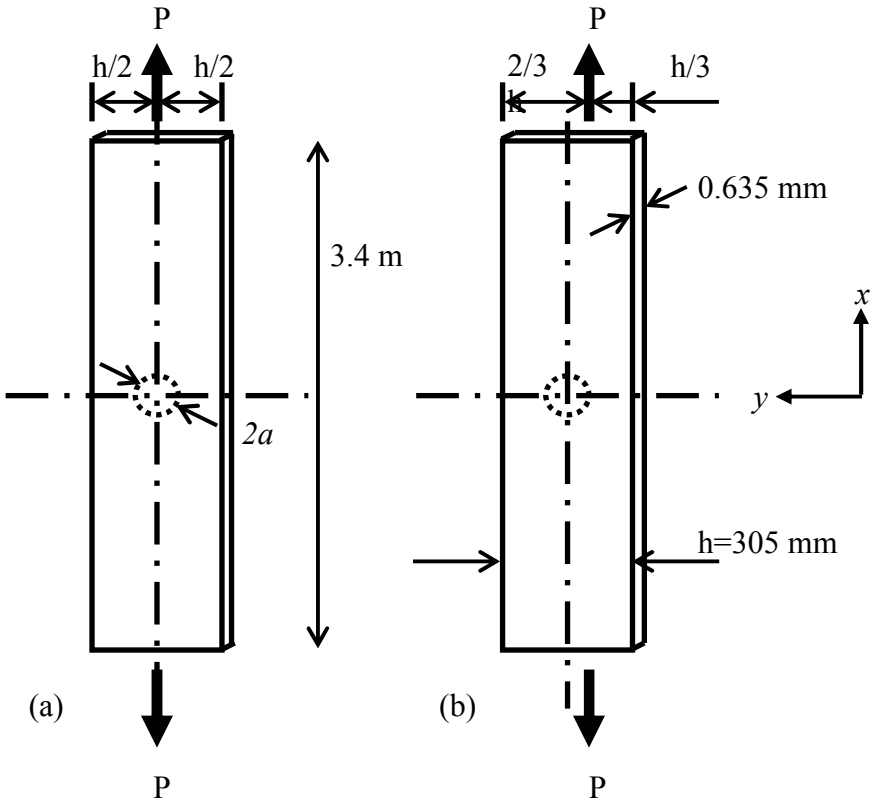

Figure 3.1: Schematic drawings of two types of test specimens: (a) Plates 1and 3 subjected to uniform normal and shear stress state; b) Plate 2 subjected to linear normal stress gradient and uniform shear stress

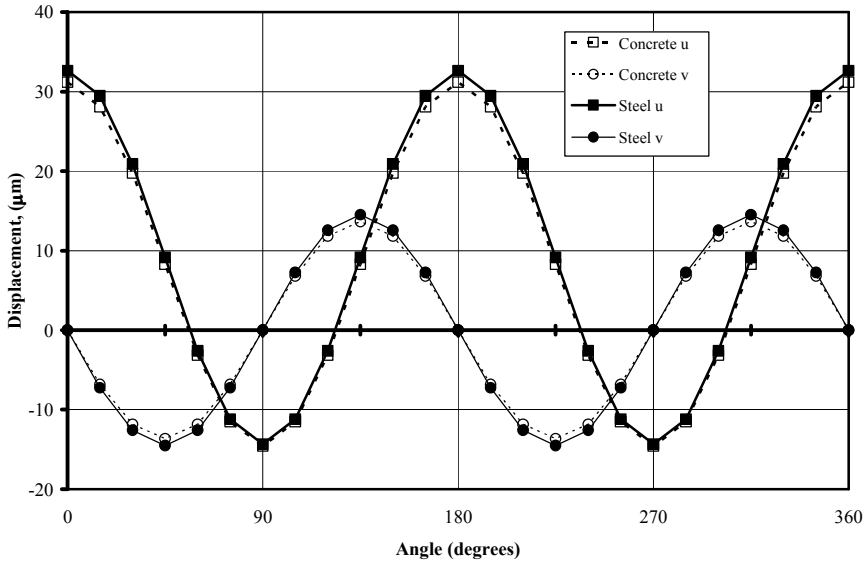

Figure 3.2: Theoretical radial (u) and tangential (v) relieved displacements for the hypothetical concrete structure and representative steel plate for the uniform stress state

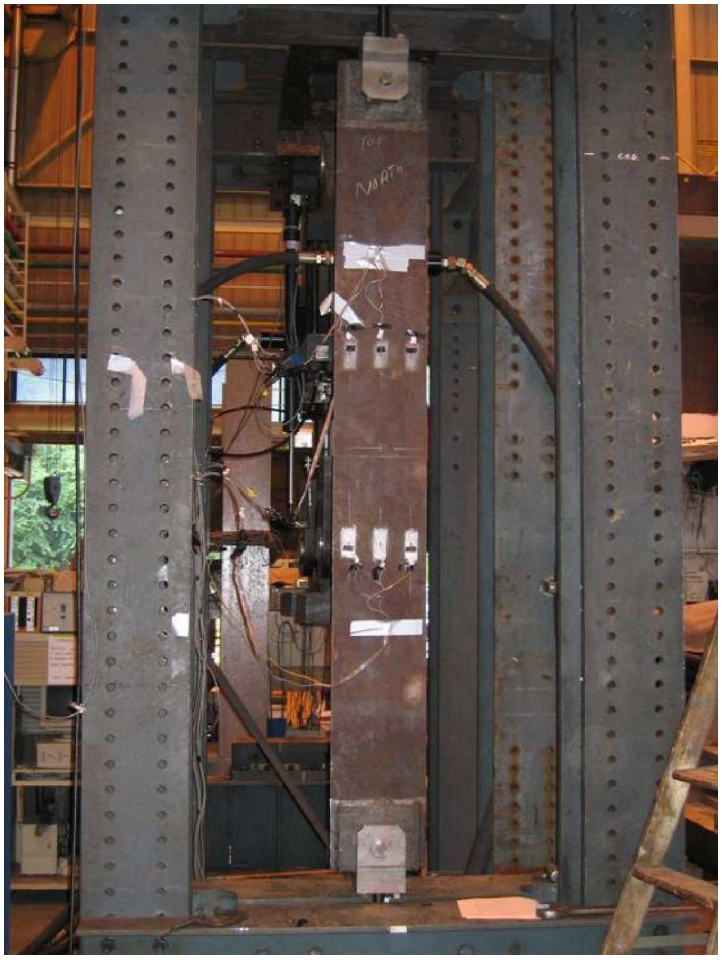

Figure 3.3: Load frame with Plate 1 positioned for testing

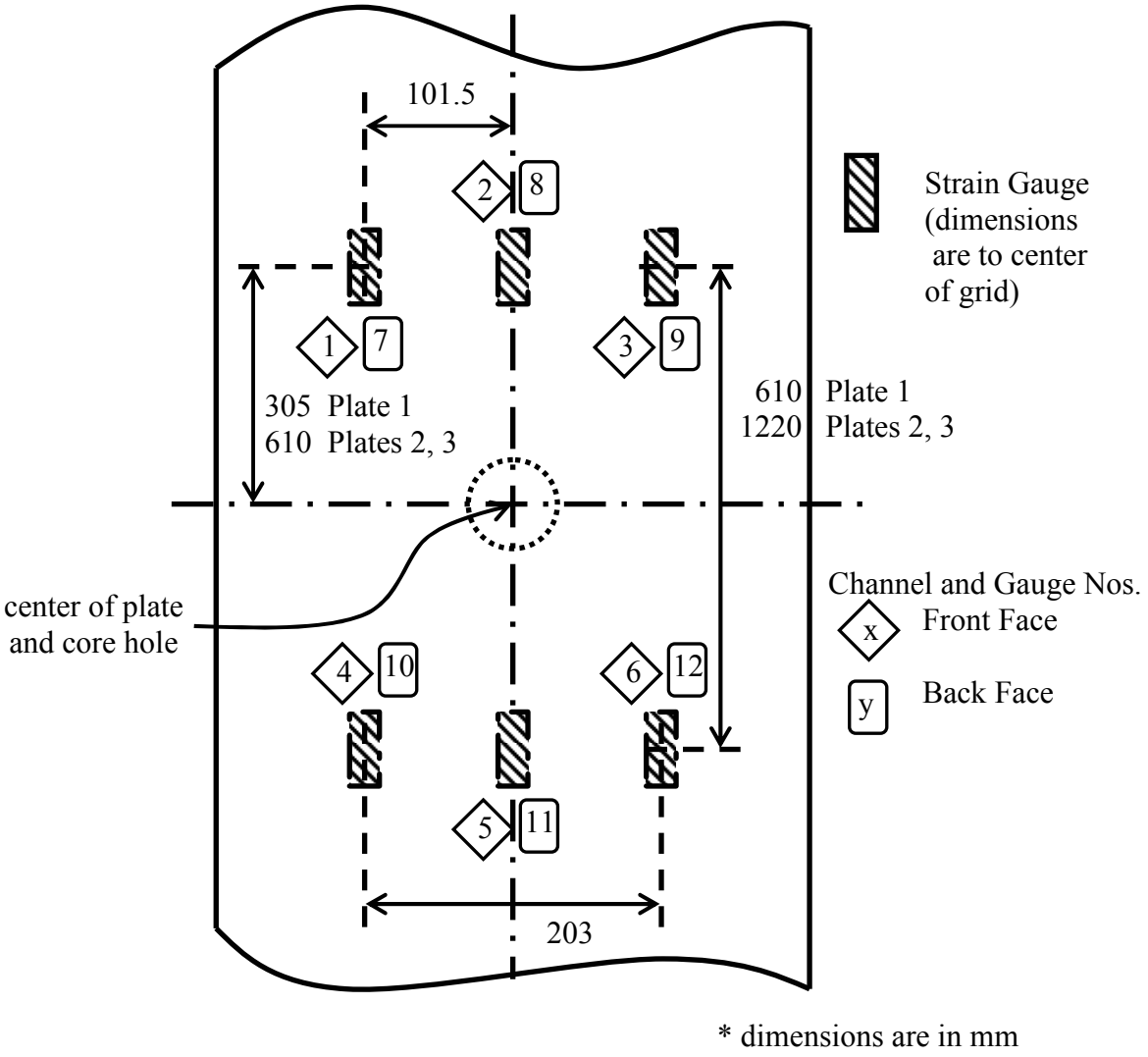

Figure 3.4 – Strain gauge layout and numbering scheme

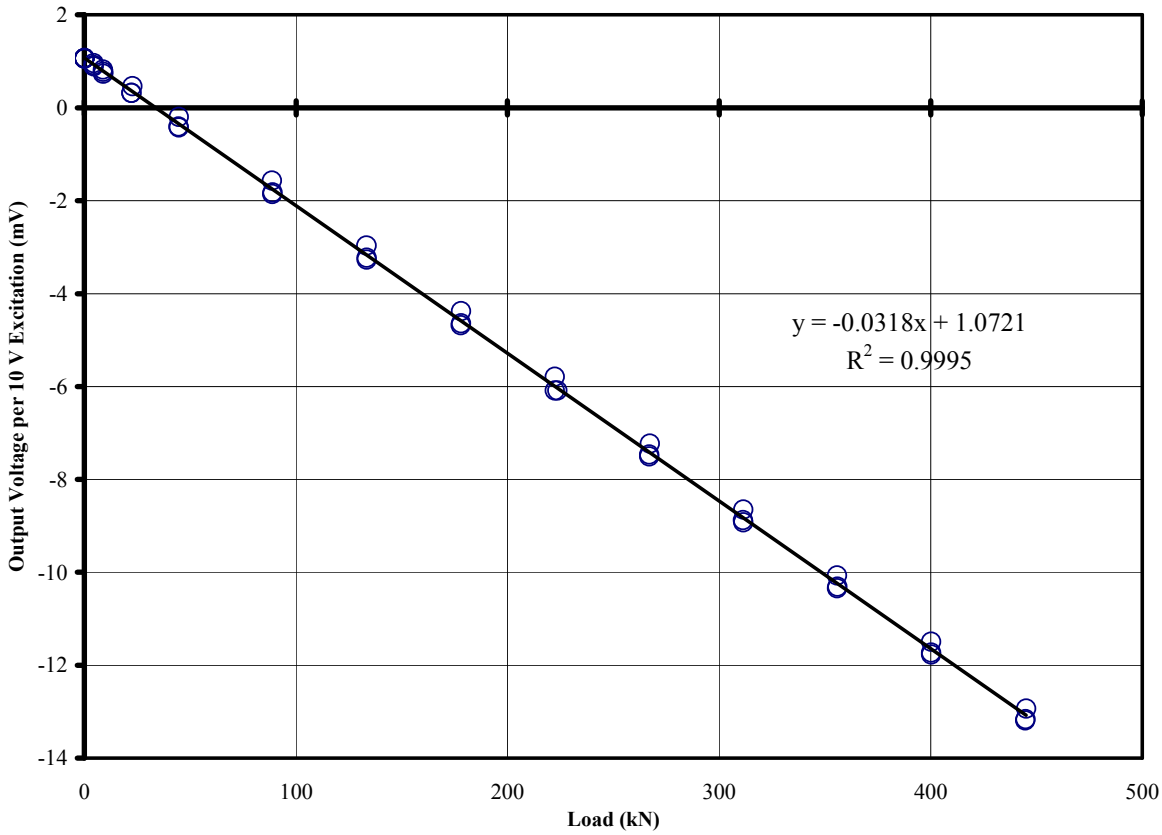

Figure 3.5: Load cell calibration data

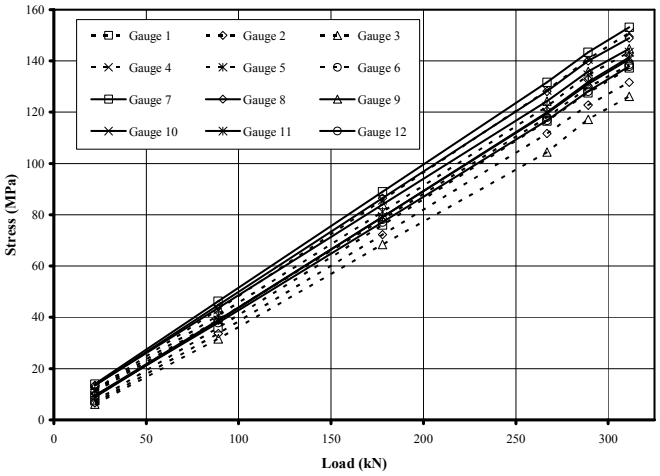

Figure 3.6: Stress versus load data for Plate 1

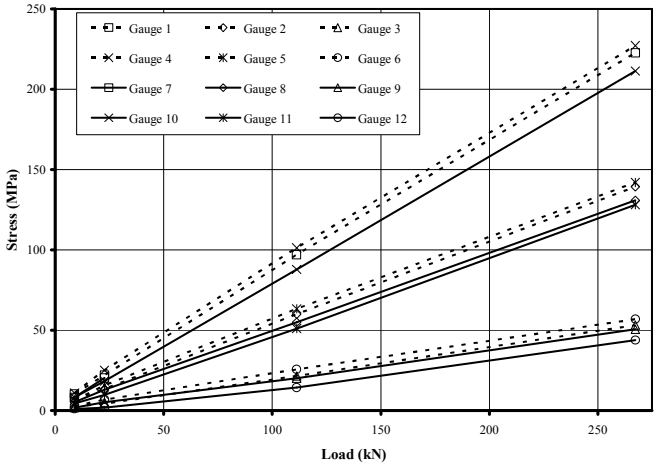

Figure 3.7: Stress versus load data for Plate 2

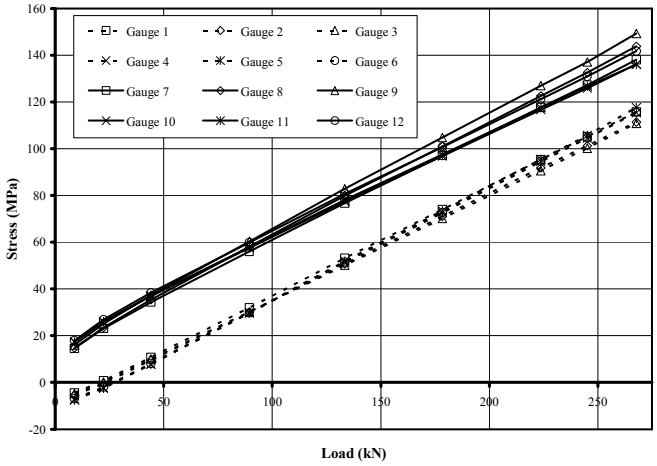

Figure 3.8: Stress versus load data for Plate 3

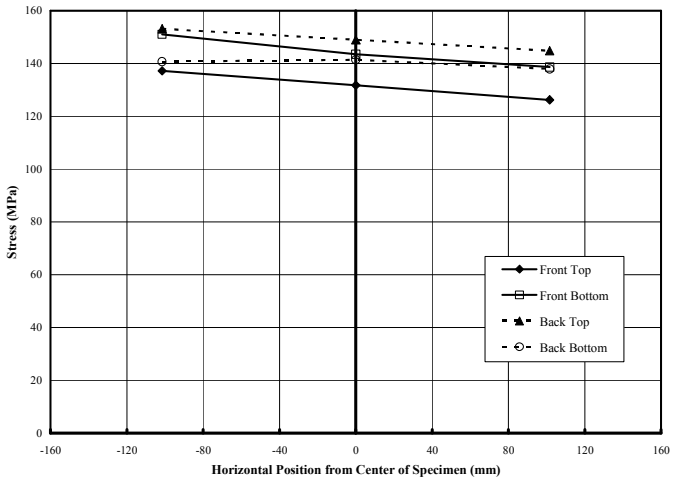

Figure 3.9: Stress profile for Plate 1

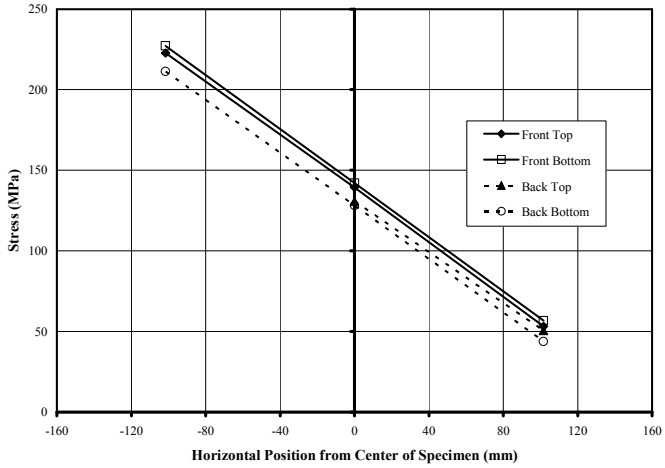

Figure 3.10 Stress profile for Plate 2

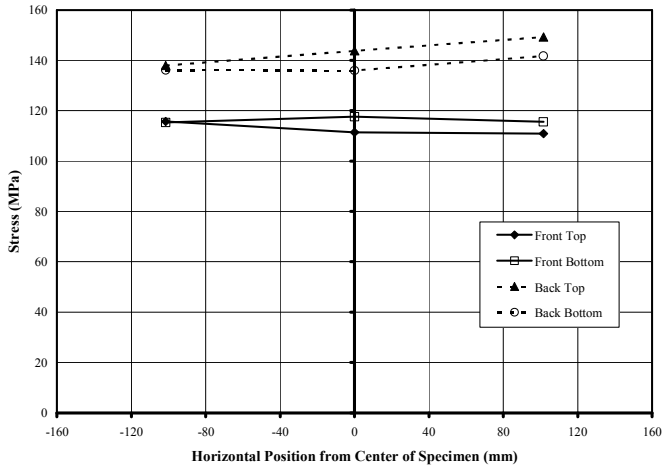

Figure 3.11: Stress profile for Plate 3

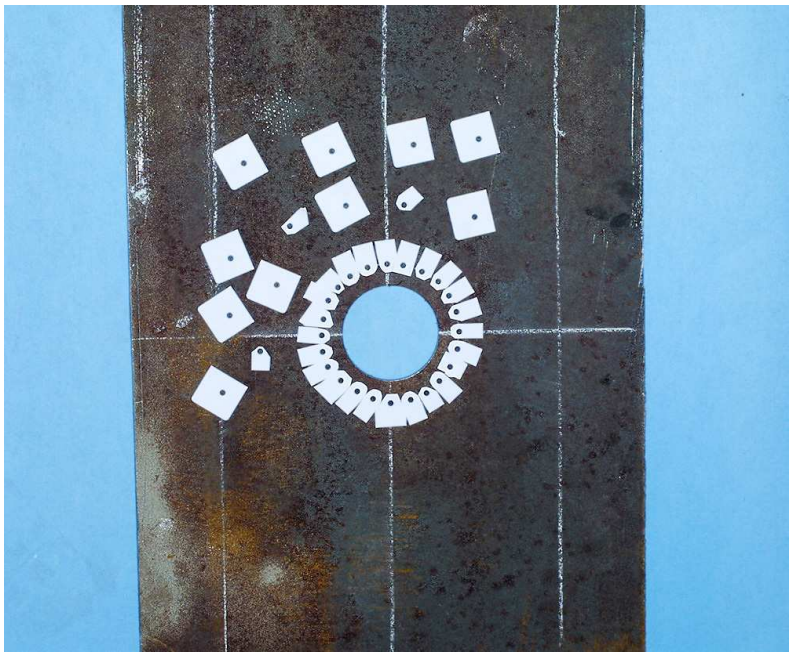

(a)

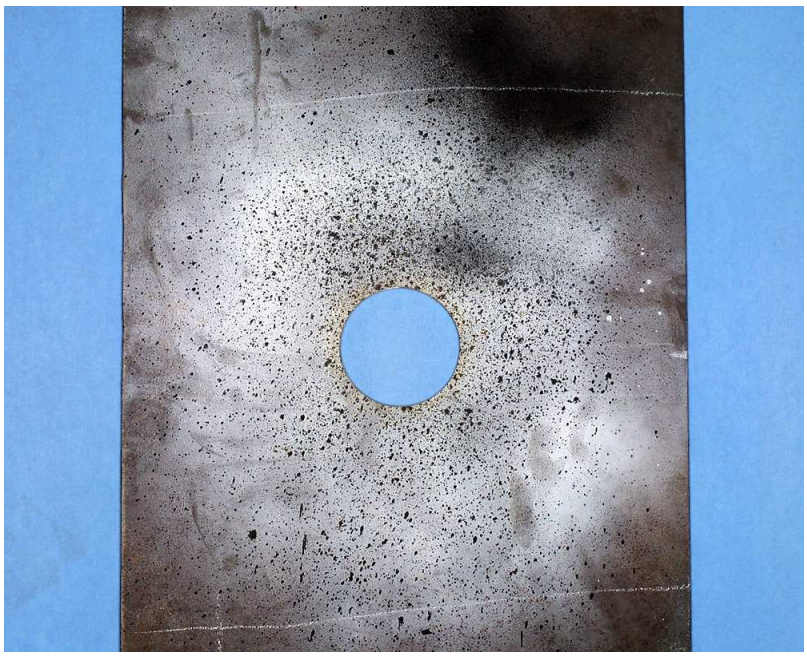

(b)

Figure 3.12: Photographs of plates after coring: (a) Plate 1 subjected to photogrammetry; (b) Plate 2 subjected to 3D Image Correlation Photogrammetry

Figure 3.13: Coring drill magnetically attached to Plate 2

(a)

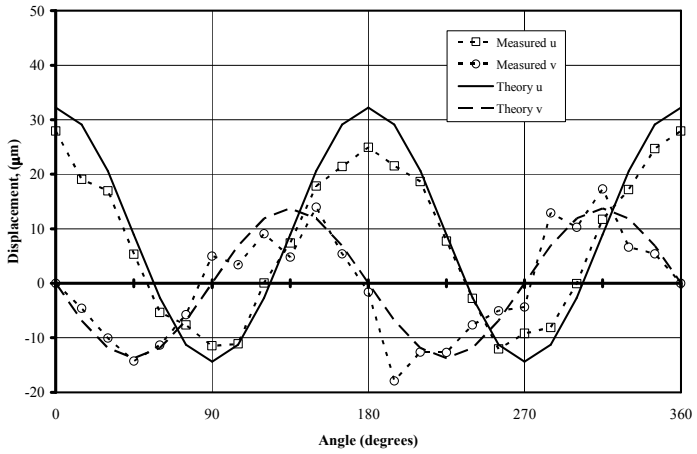

(b)

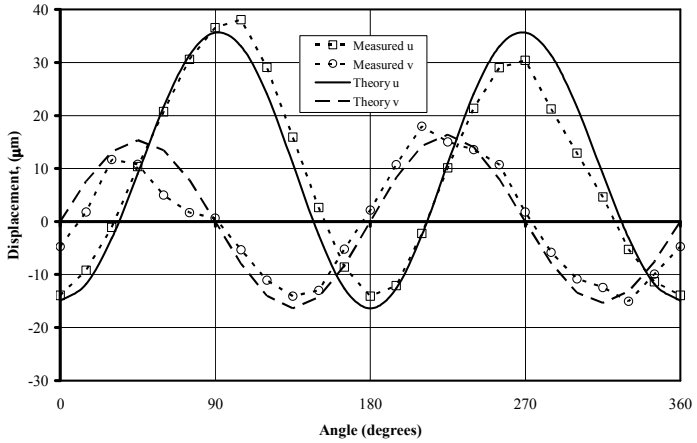

(c)

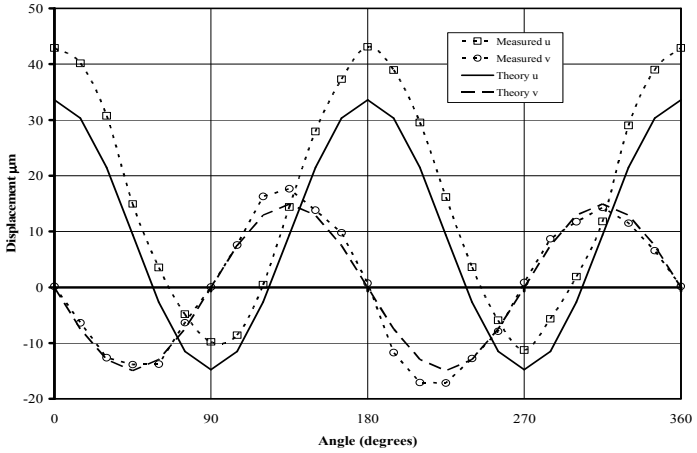

Figure 3.14: Theoretical and measured radial (*u*) and tangential (*v*) displacements from: (a) Plate 1; (b) Plate 2; and (c) Plate 3

Table 3.1 - Test matrix information

Parameter	Specimen			
	Hypothetical Concrete Structure	Plate 1	Plate 2	Plate 3
Material	concrete (f'_c=55.2 Mpa)	steel	steel	steel
a	50.8 mm	28.58 mm	31.75 mm	31.75 mm
m	76.2 mm	42.02 mm	44.45 mm	44.45 mm
P	-	289 kN	267 kN	267 kN
eccentricity	0	0	50.8 mm	0
σ_x	13.8 MPa	141.2 MPa	135.5 MPa	127.6 MPa
σ_y, τ_{xy}, K_y	0	0	0	0
K_x	0	0	0.83 MPa/mm	0

Table 3.2 - Load cell calibration data (calibration performed at 10 V excitation)

Load Cell Orientation					
0 Degrees		45 Degrees		90 Degrees	
Load (kN)	Output Voltage (mV)	Load (kN)	Output Voltage (mV)	Load (kN)	Output Voltage (mV)
0.0	1.068	0.0	1.062	0.0	1.058
4.4	0.955	4.4	0.894	4.4	0.916
8.8	0.821	8.9	0.735	8.9	0.774
22.7	0.465	22.3	0.313	22.4	0.317
44.6	-0.199	44.5	-0.408	44.6	-0.426
88.8	-1.574	88.9	-1.824	88.8	-1.855
133.3	-2.969	133.5	-3.232	133.5	-3.269
177.9	-4.378	177.9	-4.641	177.9	-4.68
222.4	-5.795	223.6	-6.085	222.4	-6.089
267.3	-7.232	266.9	-7.462	267.0	-7.505
311.4	-8.646	311.4	-8.88	311.4	-8.926
355.8	-10.069	355.9	-10.306	355.8	-10.347
400.2	-11.494	400.3	-11.729	400.2	-11.769
445.1	-12.931	444.8	-13.157	444.7	-13.193
0.0	1.065	0.0	1.061	0.0	1.061

Table 3.3 - Plate 1 strain gauge and load cell data

Load (kN)[1]	Front Face Gauges[2]						Back Face Gauges[2]					
	Gauge 1 (MPa)	Gauge 2 (MPa)	Gauge 3 (MPa)	Gauge 4 (MPa)	Gauge 5 (MPa)	Gauge 6 (MPa)	Gauge 7 (MPa)	Gauge 8 (MPa)	Gauge 9 (MPa)	Gauge 10 (MPa)	Gauge 11 (MPa)	Gauge 12 (MPa)
22.2	7.4	6.6	6.1	11.7	11.3	10.8	13.9	13.4	13.4	8.8	9.4	9.3
89.0	35.9	33.6	31.6	43.0	40.7	39.0	46.3	44.8	43.6	38.7	38.9	37.9
177.9	76.0	72.2	68.4	85.8	81.2	78.2	89.0	86.5	83.9	79.2	79.1	77.1
266.9	116.5	111.6	104.4	128.5	122.2	118.0	131.7	128.1	124.3	119.6	120.0	116.8
289.1	127.6	122.7	117.2	140.7	134.5	129.6	143.4	140.0	135.8	131.0	131.8	128.1
311.4	137.2	131.7	126.2	151.0	143.4	138.6	153.1	148.9	144.8	140.7	141.3	137.9

[1] - to convert to raw output (mV) divide by Gain = 202 and by 0.4448

[2] - to convert to raw output (mV) divide by Gain = 1414 and by 0.06895

Table 3.4 - Plate 2 strain gauge and load cell data

Load (kN)[1]	Front Face Gauges[2]						Back Face Gauges[2]					
	Gauge 1 (MPa)	Gauge 2 (MPa)	Gauge 3 (MPa)	Gauge 4 (MPa)	Gauge 5 (MPa)	Gauge 6 (MPa)	Gauge 7 (MPa)	Gauge 8 (MPa)	Gauge 9 (MPa)	Gauge 10 (MPa)	Gauge 11 (MPa)	Gauge 12 (MPa)
8.9	10.2	6.5	2.6	10.8	6.4	2.6	8.1	5.1	1.8	8.1	4.3	1.0
22.7	21.9	13.4	4.3	25.0	15.6	6.8	20.2	12.8	5.2	18.4	9.8	1.8
111.2	96.9	59.9	21.5	101.3	63.3	25.6	[d]	55.0	20.1	87.8	51.1	14.3
267.3[a]	222.0	138.6	52.9	226.2	141.3	56.5	[d]	130.5	50.3	210.3	127.4	43.5
267.3[b]	223.4	140.0	53.3	228.2	142.7	57.2	[d]	131.2	50.7	212.4	128.8	44.1
267.3[c]	222.7	139.3	53.1	227.2	142.0	56.8	[d]	130.8	50.5	211.3	128.1	43.8

[1] - to convert to raw output (mV) divide by Gain = 202 and by 0.4448

[2] - to convert to raw output (mV) divide by Gain = 1414 and by 0.06895

[a] - load and stress values *before* coring operation

[b] - load and stress values *after* coring operation

[c] - average load and stress values from [a] and [b]. These values are used elsewhere in this report when final load/stress values for Plate 2 are referenced (for example Figure 3.10 or Table 3.1).

[d] - gauges lost

Table 3.5 - Plate 3 strain gauge and load cell data

Load (kN)[1]	Front Face Gauges[2]						Back Face Gauges[2]					
	Gauge 1 (MPa)	Gauge 2 (MPa)	Gauge 3 (MPa)	Gauge 4 (MPa)	Gauge 5 (MPa)	Gauge 6 (MPa)	Gauge 7 (MPa)	Gauge 8 (MPa)	Gauge 9 (MPa)	Gauge 10 (MPa)	Gauge 11 (MPa)	Gauge 12 (MPa)
8.9	-4.4	-5.4	-4.7	-7.2	-7.5	-7.0	14.5	14.7	16.0	17.3	17.4	17.9
22.2	0.7	-0.5	0.2	-2.3	-2.6	-2.0	23.1	23.5	25.1	25.9	26.1	26.9
44.0	10.8	9.4	10.0	7.9	7.7	8.1	34.3	35.4	37.2	36.9	37.2	38.3
89.4	32.0	30.1	30.2	29.6	29.9	29.8	56.0	58.1	60.3	57.5	57.8	59.9
133.4	53.2	50.7	50.1	51.4	51.9	51.5	76.7	79.9	82.9	77.4	78.1	80.6
178.4	73.9	71.0	70.1	72.6	73.4	72.7	97.0	101.0	104.7	96.8	97.6	100.7
223.7	95.4	91.8	90.6	94.5	95.5	94.6	117.6	122.6	126.9	116.7	117.5	121.3
245.1	105.2	101.2	100.2	104.5	105.7	104.6	127.2	132.5	137.1	125.8	126.7	130.9
267.3[a]	115.8	111.7	110.3	115.1	116.6	115.4	137.3	143.4	148.2	135.7	136.6	141.3
268.2[b]	115.7	111.1	111.5	115.5	118.6	115.8	138.6	144.1	150.3	136.6	135.3	142.0
267.8[c]	115.8	111.4	110.9	115.3	117.6	115.6	138.0	143.8	149.3	136.1	136.0	141.7

[1] - to convert to raw output (mV) divide by Gain = 202 and by 0.4448

[2] - to convert to raw output (mV) divide by Gain = 1414 and by 0.06895

[a] - load and stress values *before* coring operation

[b] - load and stress values *after* coring operation

[c] - average load and stress values from [a] and [b]. These values are used elsewhere in this report when final load/stress values for Plate 3 are referenced (for example Fig. 3.11 or Table 3.1).

Table 3.6 - Experimental results for Plates 1, 2 and 3

Specimen	Measured Quantity	Stress Results	
		Magnitude (MPa or MPa/mm)	Percentage Difference from Applied σ_x or K_x
Plate 1 photogrammetry	σ_x	117.4	-16.9
	σ_y	4.6	3.3
	τ_{xy}	6.5	4.6
Plate 2 3D Image Correlation Photogrammetry	σ_x	126.3	-6.8
	σ_y	6.9	5.1
	τ_{xy}	1.2	0.9
	K_x	0.56	-32.5
Plate 3 3D Image Correlation Photogrammetry	σ_x	174.3	36.6
	σ_y	38.9	30.5
	τ_{xy}	1.9	1.5

CHAPTER 4

REFERENCES

1. Pessiki, S., Turker, H., "Theoretical Formulation of the Core Drilling Method to Evaluate Stresses in Concrete Structures," Review of Progress in Quantitative Nondestructive Evaluation, D. O. Thompson and D. E. Chimenti (Editors), American Institute of Physics, 1731-1737 (1999).

2. Turker, H., Pessiki, S., "Theoretical Development of the Core-Drilling Method for Nondestructive Evaluation of Stresses in Concrete Structures," Report No. 03-07, Center for Advanced Technology for Large Structural Systems, Lehigh University, 300 pp. (2003).

3. Schajer, G. S., "Application of Finite Element Calculations to Residual Stress Measurements," Journal of Engineering Materials and Technology, **103** (2), 157-163 (1981).

4. Schajer, G. S., "Measurement of Non-uniform Residual Stresses Using the Hole-Drilling Method. Part I," Transactions of ASME, **110** (4), 338-343 (1988).

5. Schajer, G. S., "Measurement of Non-uniform Residual Stresses Using the Hole-Drilling Method. Part II," Transactions of ASME, **110** (4), 344-349 (1988).

6. Beghini, M., "Recent Advances in the Hole Drilling Method for Residual Stress Measurement," Journal of Materials Engineering and Performance, **7** (2), 163-172 (1998).

7. Beghini, M., "Analytical Expression of the Influence Functions for Accuracy and Versatility Improvement in the Hole-Drilling Method," Journal of Strain Analysis, **35** (2), 125-135 (2000).

8. Flaman, M.T., "Determination of Residual Stress Variation with Depth by the Hole-Drilling Method," Experimental Mechanics, **25** (9), 205-207 (1985).

9. Schajer, G.S., Yang, L. "Residual-Stress Measurement in Orthotropic Materials Using the Hole-Drilling Method," Experimental Mechanics, **34** (4), 324-333 (1994).

10. Tyson, J., Schmidt, T., Galanulis, K., "Advanced Photogrammetry for Robust Deformation and Strain Measurement," Proceedings of SEM 2002 Annual Conference, Milwaukee, WI, (2002).

11. Muskhelishvili, N. I., Some Basic Problems of the Mathematical Theory of Elasticity, Fourth Corrected and Augmented Edition, J. R. M. Radok (trans), P. Noordhoff Ltd. Groningen, Netherlands, 718 pp. (1954).

12. Merkhar-Asl, S. "Concrete stress-relief coring: theory and practice," First Symposium on Post-Tensioned Concrete Structures, FIP Conference – London, 569-576 (1996).

13. Owens, A. "In-situ stress determination used in structural assessment of concrete structures," Strain, **29** (4), 115-123 (1993).

14. Schajer, G. S., Steinzig, M. "Full-Field Calculation of Hole-Drilling Residual Stresses from ESPI Data," Experimental Mechanics, in review.